energies

MDPI

Article

Assessing the Limits of Equivalent Circuit Models and Kalman Filters for Estimating the State of Charge: Case of Agricultural Robots

German Monsalve [1], Alben Cardenas [1,*], Diego Acevedo-Bueno [1] and Wilmar Martinez [2]

[1] Electrical and Computer Engineering Department, University of Quebec at Trois-Rivieres, 3351, Boulevard des Forges, Trois-Rivieres, QC G8Z 4M3, Canada
[2] Department of Electrical Engineering (ESAT), KU Leuven—EnergyVille, Thor Park 8310-bus 12135, 3600 Genk, Belgium
* Correspondence: alben.cardenasgonzalez@uqtr.ca

Abstract: The battery State of Charge (SoC) is critical information to overcome agricultural robots' limitations related to battery and energy management. Although several SoC estimation methods have been proposed in the literature, the performance of these methods has not been validated for different battery chemistries in agricultural mobile robot applications. Compared to previous work, this paper evaluates the limits of the SoC estimation using the RC model and the Thevenin model for a Lithium Iron Phosphate (LFP) battery and a Sealed Lead Acid (SLA) battery. This evaluation used a custom agricultural robot in a controlled indoor environment. Consequently, this work assessed the limitations of two ECM-based SoC estimation methods using battery packs, low-cost sensors and discharge cycles typically used in agricultural robot applications. Finally, the results indicate that the RC model is not suitable for SoC estimation for LFP battery; however, it achieved a mean absolute error (MAE) of 2.2% for the SLA battery. On the other hand, the Thevenin model performed properly for both chemistries, achieving MAE lower than 1%.

Keywords: state of charge estimation; lithium iron phosphate; sealed lead acid; RC model; Thevenin model; agricultural robots

Citation: Monsalve, G.; Cardenas, A.; Acevedo-Bueno, D.; Martinez, W. Assessing the Limits of Equivalent Circuit Models and Kalman Filters for Estimating the State of Charge: Case of Agricultural Robots. *Energies* **2023**, *16*, 3133. https://doi.org/10.3390/en16073133

Academic Editors: Jarosław Konieczny and József Vásárhelyi

Received: 6 March 2023
Revised: 24 March 2023
Accepted: 28 March 2023
Published: 30 March 2023

1. Introduction

The growing demand for food and the mitigation of the effects of climate change are leading to profound transformations in agricultural production. In this context, agricultural production should be oriented towards practices and technologies with low greenhouse gas emissions and high efficiency in the use of water and pesticides [1–3]. Furthermore, a high degree of automation must be incorporated into new agricultural solutions due to labor shortages, especially in developed countries [4,5].

Battery-powered agricultural robots could provide a solution to increase farms' productivity sustainably. In addition, agricultural robots can reduce the use of pesticides and fertilizers, allowing farmers to optimize their resources and increase productivity [6]. Moreover, autonomous robots designed for precision agriculture can help workers in tasks like weeding and seeding, offering a solution to labor shortage problems [7].

Nevertheless, more technological advances and research are needed in battery and energy management to enlarge the application of robots on farms [8,9]. The battery State of Charge (SoC) is essential information for the Battery Management System (BMS) and the robot's energy management. Therefore, the SoC can optimize the battery charging process and operation of robots. Moreover, the BMS uses the battery SoC to avoid overcharge and overdischarge, which can lead to electrolyte decomposition, capacity fade, battery impedance increase, thermal runaway and fire [10,11]. However, one of the main challenges

of obtaining the SoC is that it cannot be measured directly; instead, it must be estimated using voltage, current, temperature and aging during operation [12].

Although SoC estimation methods usually use some or all of the parameters mentioned above, each type of battery (chemistry) presents an Open-Circuit Voltage (OCV) vs. SoC characteristic curve. Thus, the studies performed for lithium nickel–manganese–cobalt oxide or lithium nickel–cobalt–aluminium oxide batteries, which are widely used in Electric Vehicles (EVs), cannot be directly extrapolated for their application in mobile robots. Sealed Lead Acid (SLA) or Lithium Iron Phosphate (LFP) battery packages are preferred for agricultural robots because of their lower price and low fire risk. For instance, SoC estimation of LFP batteries represents a significant challenge due to its flat OCV vs. SOC relationship. In addition, agricultural robots are low-cost devices with small battery packs and tight hardware resources, particularly low-end microcontrollers and low-precision current and voltage sensors. This leads to SoC estimation methods offering low performance.

Several conventional methods have been proposed to estimate the SoC of batteries. For instance, the Coulomb counting method is a conventional online method that measures the amount of charge transferred to and from the battery. However, this method is affected by measurement errors, internal battery losses and the self-discharging phenomena, which reduces the SoC estimation accuracy over time [13]. Therefore, unless providing some feedback mechanism, the Coulomb counting method is impractical for estimating the SoC [14]. Another approach is the OCV method, which performs an offline SoC estimation using the relationship between the battery's OCV and SoC. Nevertheless, this method requires that the battery reaches a stable state requiring long rest time (over an hour).

Furthermore, several data-driven methods have been presented in the last ten years. These methods are based mainly on Artificial Neural Networks (ANN), which employ data from previous battery tests to model the battery behavior and estimate the SoC. To obtain a consistent estimation, these ANNs require long training periods using high-performance specialized processors and large datasets [15–17]. In general, the ANN accuracy was validated through simulations using several driving cycles of EVs. Considering these particularities, this approach is unfeasible for low-cost agricultural robots.

In addition, the SoC of batteries can also be estimated using model-based methods that use an Electrical Circuit Model (ECM) and a state observer like the Kalman Filter (KF) [18], the Extended Kalman Filter (EKF) [18–20] or the Unscented Kalman Filter (UKF) [21]. ECMs consist of a circuit containing resistors, capacitors and voltage sources that models the battery behavior. The RC model and the Thevenin model are among the most popular ECMs. These methods offer an online high-accuracy SoC estimation and overcome the limitations of the Coulomb counting method [22,23]. The performance of these methods depends primarily on the accuracy of the model. However, a trade-off must be found between the complexity of the model, the computational cost and the accuracy of the model and SoC estimation, especially under cost and hardware constraints, as in the case of low-cost embedded systems [24].

1.1. Related Work

Several SoC estimation methods based on ECM have been developed in recent years. In [24], the state of charge of a battery cell for electric vehicles was estimated using an adaptive EKF and the performance of the estimation was validated under EV drive cycle tests conducted using a BTS-5V300A battery test bench. In [22], the SoC of a battery pack intended for EV applications was estimated using the Luenberger observer. A Digatron battery testing system, BTS-600, was used to perform the battery tests. Another ECM-based SoC estimation for EV batteries is presented in [25], where the estimation is performed using the UKF. The battery was discharged using a programmable electronic load, EL-9000 and a data acquisition unit NI-9229 and the computation of the estimation was executed in Labview. A hybrid approach that combines Coulomb counting, OCV method and a model-based approach was presented in [26]. The authors cycled a Lithium Manganese Oxide (LMO) battery cell using the SBT0550 battery testbench using EV drive cycles. In

general, the methods presented before were intended for EV applications. Moreover, the validation was performed using specialized laboratory equipment and EV drive cycles to discharge the battery. Therefore, the effects of noise and uncertainty were not evaluated and the limitations of agricultural robots were not considered.

For low-cost mobile robots, few SoC estimation methods have been implemented and validated. For example, in [21], the parameters of the RC model and SoC of the battery pack were estimated using the UKF and the EKF, respectively. The proposed SoC estimation approach was validated using a mobile robotic platform in a laboratory environment in a narrow SoC band (90–98%). In [27], the SoC estimation for a transmission lines inspection robot was performed adopting an RC model, whose parameters were obtained offline. Then, the SoC estimation was obtained using the H∞ observer. The accuracy of this work was validated only for a restricted range varying from 68% to 65% SoC. Considering the limited range evaluated in these studies, there is a need to assess the performance of SoC estimation methods designed for robots using different battery chemistries over a broader range of SoC. Table 1 compares the previous SoC estimation methods in the literature review with the presented research work.

As a result of the literature review, the following limitations were identified:

- Few studies focused on the limitations and challenges of SoC estimation for mobile robots, specifically for agricultural robots.
- SoC estimation methods for robotic applications were validated in a narrow SoC range.
- Previous work has not considered the performance of the ECM-based SoC estimation method using low-cost equipment and batteries typically used in robot applications.

Table 1. Comparison of presented work with previous research.

Ref.	Battery	Equivalent Circuit Model	Convergence Test	Low Cost Equipment	SoC Validation Range	Validation Test
[21]	37 V 8 Ah Li-ion Battery Pack	RC model	No	No	98% to 90%	Robot discharge cycles
[27]	25 V 18 Ah Li-ion Battery Pack	RC model	No	Yes	68% to 65%	Robot discharge cycles
[24]	3.7 V 35 Ah Li-ion Battery Cell	Thevenin model	Yes	No	100% to 20%	EV drive cycle
[22]	56 V 105 Ah Battery Pack	RC model	No	No	90 to 10%	EV drive cycles
[25]	3.6 V 3.3 Ah LFP Battery Cell	Thevenin model	Yes	No	100% to 20%	EV drive cycles
[26]	4.2 V 15 Ah Lithium Manganese Oxide Battery Cell	Thevenin model	No	No	70% to 65%	EV drive cycles
This work	12 V 5 Ah SLA Battery Pack and 12 V 6 Ah LFP Battery Pack	RC model and Thevenin model	Yes	Yes	100% to 60% 100% to 20%	Agricultural Robot discharge cycles

1.2. Contributions and Organization

Since the performance of an SoC estimation method is application dependent [28], it is important to evaluate the limitations of the SoC estimation in an agricultural robot application using battery packs instead of battery cells. Therefore, this paper provides an analysis of the limits of two model-based SoC estimation methods for LFP and SLA 12 V battery packs, which are commonly used in agricultural robot platforms. The two methods analyzed are the RC model with KF and the 2 RC Thevenin model with UKF, which have been used to estimate the SoC of battery cells for EVs [18,19]. This work evaluates the performance of these models by using a custom agricultural robot, presented in Figure 1. The methods were assessed in a broad range of SoC, from 100% SoC to the lower limit recommended by the manufacturer, i.e., the maximum range of discharge. The results of this paper can be used by designers to choose the correct SoC estimation method for a particular low-cost mobile robot and battery chemistry.

The remainder of this paper is organized as follows. First, it introduces the RC ECM and the Thevenin ECM in Section 2. Then, SoC estimation implementation for each model is presented in Section 3. The results of the SoC estimation are presented in Section 4. Finally, the concluding remarks of this work are provided in Section 5.

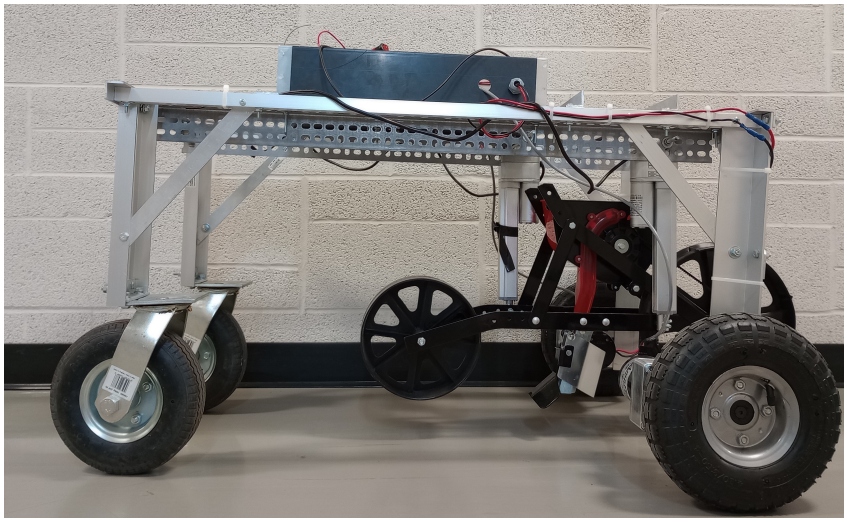

Figure 1. Agricultural robot developed at the University of Quebec at Trois-Rivières.

2. Equivalent Circuit Model Parameter Estimation

The main advantage of using equivalent circuit models is their simplicity, which allows the implementation of these approaches using low-cost hardware like microcontrollers. Moreover, using these techniques, the drawbacks of conventional and data-driven methods can be improved [28].

Previous research has demonstrated that the SoC estimation can be affected by the accuracy of the battery model. Therefore, good accuracy is needed to improve the performance of the SoC estimation process [29].

2.1. Battery Characterization Tests

This study used a 12 V 5 Ah SLA battery and a 12 V 6 Ah LFP battery. These batteries were tested using a sequence of discharge pulses followed by a one-hour relaxation period to ensure the batteries reached stable states to obtain the initial parameters of the equivalent circuit models analyzed in this study. This test aims to characterize the battery's dynamic and the relationship between the battery's OCV and the SoC. Pulse discharge tests have been used to estimate the parameter of the ECM in several previous works [18–20,27]. Figure 2 shows a detailed explanation of each section of the test pulse. For the lead-acid battery, seven pulses were applied to discharge the battery from 100% SoC to 40% SoC. Lead-acid batteries should not be discharged more than 40% SoC to increase the battery lifetime. During each pulse, the SLA battery was connected to 13.5 Ohms resistance for 30 min, then disconnected for 1 h until the next pulse. In the same way, the LFP battery was connected to a 12 Ohms resistance to discharge the battery from 100% SoC to 16% SoC. The resistance values were selected to discharge the battery 10% after each pulse. Figure 3a and Figure 3b show the characterization tests performed on the SLA battery and the LFP battery, respectively.

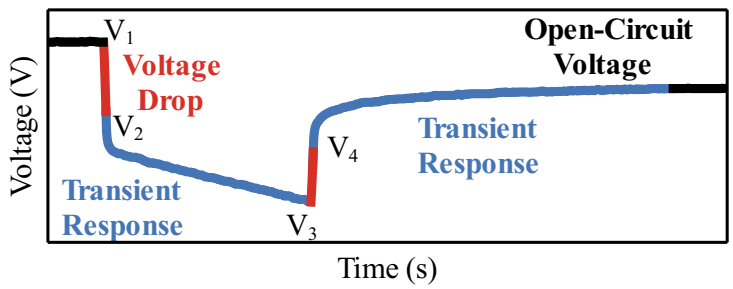

Figure 2. Explanation of a single pulse of the pulse discharge characterization test.

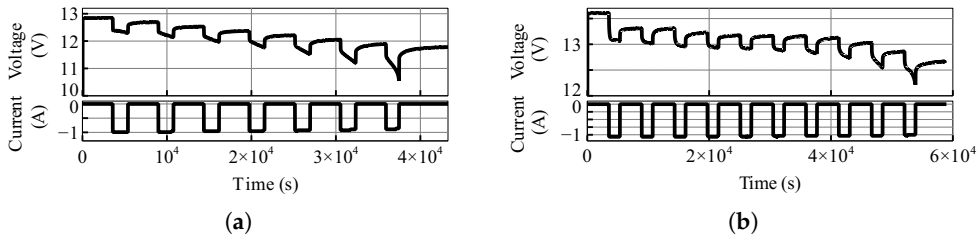

Figure 3. Pulse discharge test data from the batteries used in this work: (**a**) SLA battery pack. (**b**) LFP battery pack.

2.2. RC Model—Offline Parameter Estimation

This ECM has been proposed by Saft [30]. Prior studies have used the RC model for SoC estimation [18,27]. Figure 4a shows the RC model used in this study. This model consists of a terminal resistance and two RC branches. The terminal resistance, R_t, models the voltage drop presented when a load is connected to the battery. The surface capacitor, C_s, and the surface resistance, R_s, model the battery's surface and diffusion effects. The second RC branch contains the bulk capacitor, C_b, and bulk resistance, R_b. The bulk capacitor models the storage capacity of the battery; therefore, it is larger than the surface capacitor. Moreover, the voltage across the bulk capacitor V_{cb} represents the battery's OCV. Then, by estimating the V_{cb}, the SoC of the battery can be estimated.

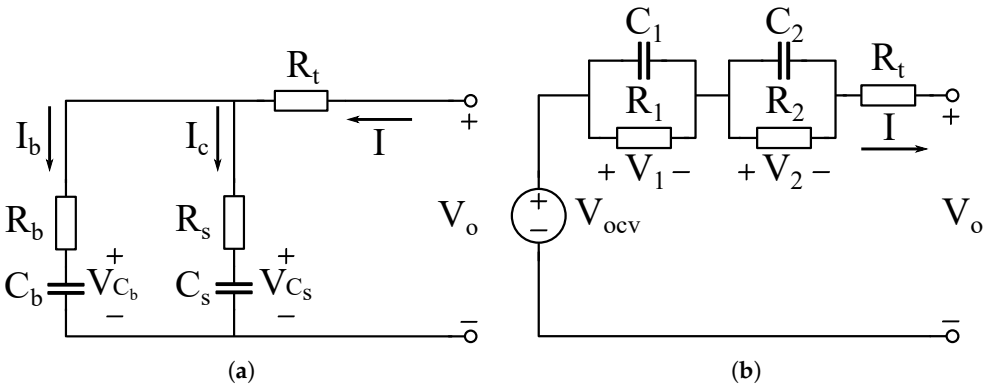

Figure 4. (**a**) RC Equivalent Circuit Model [30]. (**b**) Thevenin Equivalent Circuit Model [31].

The RC model can be represented using the following state-space representation:

$$\begin{bmatrix} \dot{V}_{cb} \\ \dot{V}_{cs} \\ \dot{V}_o \end{bmatrix} = \begin{bmatrix} -\frac{1}{C_b(R_b+R_s)} & \frac{1}{C_b(R_b+R_s)} & 0 \\ \frac{1}{C_s(R_b+R_s)} & -\frac{1}{C_s(R_b+R_s)} & 0 \\ A_{3,1} & 0 & A_{3,3} \end{bmatrix} \begin{bmatrix} V_{cb} \\ V_{cs} \\ V_o \end{bmatrix} + \begin{bmatrix} \frac{R_s}{C_b(R_b+R_s)} \\ \frac{R_b}{C_s(R_b+R_s)} \\ B_{3,1} \end{bmatrix} [I] \quad (1)$$

$$[V_o] = \begin{bmatrix} 0 & 0 & 1 \end{bmatrix} \begin{bmatrix} V_{cb} \\ V_{cs} \\ V_o \end{bmatrix} \quad (2)$$

$$A_{3,1} = -\frac{R_s}{C_b(R_b+R_s)^2} + \frac{R_b}{C_s(R_b+R_s)^2} - \frac{R_s^2}{C_bR_b(R_b+R_s)} + \frac{R_s}{C_s(R_b+R_s)^2} \quad (3)$$

$$A_{3,3} = \frac{R_s}{C_bR_b(R_b+R_s)} - \frac{1}{C_s(R_b+R_s)} \quad (4)$$

$$B_{3,1} = \frac{R_b^2}{C_s(R_b + R_s)^2} - \frac{R_s R_s}{C_b R_b (R_b + R_s)} + \frac{R_t}{C_s(R_b + R_s)} + \frac{R_s R_b}{C_s(R_b + R_s)^2} \quad (5)$$

where I is the battery's current and V_o is the battery's terminal voltage. V_{cb} and V_{cs} are the voltage of the bulk capacitor and surface capacitor, respectively.

The battery characterization tests are used to obtain the initial parameters of the equivalent circuit model and the OCV vs. SoC curve by analyzing the test data as proposed in [18,27]. The battery's total resistance can be found by examining the instantaneous response of the battery. The voltage difference ($V_1 - V_2$ from Figure 2) and the current pulse magnitude are used to calculate the battery's resistance value using the following expression:

$$R_{total} = \frac{V_2 - V_1}{I_{pulse}}. \quad (6)$$

According to [18], the bulk and surface resistance values are equal to 75% of the battery's total resistance:

$$R_b = R_s = 0.75 * R_{total}. \quad (7)$$

After finding R_b and R_s, the terminal resistance R_t can be obtained using the following expression:

$$R_t = R_{total} - \frac{R_b}{2}. \quad (8)$$

The first 500 ms of each pulse are analyzed to obtain the value of the surface capacitor C_s. Then, the time constant of the surface capacitor is obtained by performing a curve fitting using the MATLAB fit function:

$$V_{start} + (V_{end} - V_{start}) * (1 - \exp(-x/\tau)). \quad (9)$$

where V_{start} is the battery's voltage before the beginning of the current; V_{end} is the voltage after 500 ms without load. Then, using the time constant τ obtained from the curve fitting, C_s can be found as follows:

$$C_s = \frac{\tau}{2R_s}. \quad (10)$$

2.3. Thevenin—Offline Parameter Estimation

The second equivalent circuit model implemented in this study was the Thevenin model, which has been widely used in several research articles in the last five years [25,26,32–34]. The Thevenin model is shown in Figure 4b; the circuit has a terminal resistance R_t to model the voltage drop when a load is connected to the battery. Moreover, it has one or more parallel RC branches (from R_1C_1 to R_nC_n) connected in series to model the diffusion effects of the battery. This model has a voltage source that depends on the battery's SoC to model the OCV of the battery. The addition of the dependent voltage source makes this model nonlinear; then, a nonlinear KF is needed to estimate the SoC of the battery, adding computational complexity.

The complexity of this model can be minimized by reducing the number of RC circuits. To illustrate this, Figure 5 compares a curve fitting with one and two time constants. Two RC circuits were used in this study because this provides a good trade-off between accuracy and complexity.

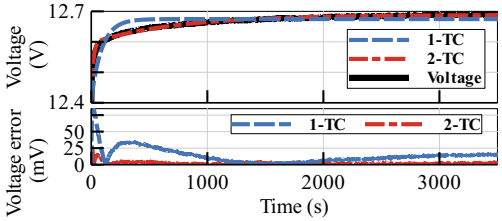

Figure 5. Performance comparison of one and two RC time constants.

The behavior of this model can be described using the following equations:

$$\dot{SoC} = -\frac{\eta I}{Q} \tag{11}$$

$$\dot{V}_1 = -\frac{V_1}{R_1 C_1} + \frac{I}{C_1} \tag{12}$$

$$\dot{V}_2 = -\frac{V_2}{R_2 C_2} + \frac{I}{C_2} \tag{13}$$

$$V_o = V_{ocv}(SoC) - V_1 - V_2 - IR_t \tag{14}$$

where η is the Coulomb efficiency, also called charging efficiency. The charging efficiency is assumed to be 1 when the battery discharges [35]. V_1 and V_2 are the voltages of the first and second RC circuits, respectively. V_o is the battery terminal voltage. I is the input current. For this model, the discharge current is positive and the charge current is negative. V_{ocv} is the battery OCV, which is a function of the battery's SoC. Therefore, this model is not linear because the V_{ocv} is a function of one of the system states, then this model can be represented with a nonlinear vector function:

$$\mathbf{x}_k = f(\mathbf{x}_{k-1}, \mathbf{u}_{k-1}) \tag{15}$$

$$\mathbf{y}_k = h(\mathbf{x}_k, \mathbf{u}_k). \tag{16}$$

Then, to estimate the SoC using the Thevenin model, a nonlinear KF such as the EKF or UKF must be selected.

An initial estimation is performed with MATLAB and Simulink using a curve fit and linear least square tools. For the estimation, each pulse of the battery characterization test is analyzed separately and used to extract a set of parameters, as presented in [19]. Since the battery is assumed to reach a stable state right before each pulse, the OCV vs. SoC curve can be obtained using the voltage value before the beginning of each pulse. Moreover, the model's terminal resistance can be calculated by measuring the voltage when a pulse is imposed on the battery. Equation (17) shows the expression used to find the battery model's terminal resistance R_t:

$$R_t = \frac{V_2 - V_1}{I_{pulse}}. \tag{17}$$

After each pulse, there is a relaxation period of 1 h; this section of the test can be used to obtain the time constants of the model. These time constants were obtained by performing a curve fit using (18), as shown in Figure 6.

$$V_o = V_{start} + V_1 e^{-\frac{t}{\tau_1}} + V_2 e^{-\frac{t}{\tau_2}} - V_1 - V_2. \tag{18}$$

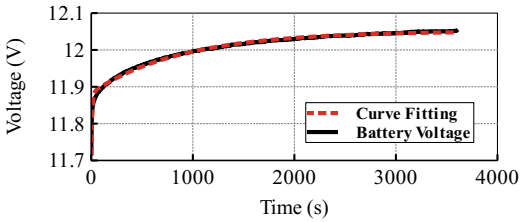

Figure 6. Curve Fitting performed to estimate the time constants of the 2RC Thevenin model for the SLA battery.

The resistances and capacitances (R_1C_1 and R_2C_2) were calculated using the linear least-squares function (lsqlin) in MATLAB. The lsqlin function estimates the model's parameters to minimize the error between the terminal voltage measurement. The results of the initial parameter estimation are shown in Figure 7a. This initial set of parameters can be refined using the nonlinear least-squares (lsqnonlin) solver, of Simulink Design

Optimization Toolbox, to perform a data fitting of the nonlinear data. The initial parameter estimation aims to avoid local minima during the optimization process. Each pulse was analyzed separately to reduce the complexity of the optimization problem. Figure 7b shows the battery voltage simulation with the final parameters estimated. At lower SoC levels, the model error increases because the diffusion and surface effects are accentuated and the 2 RC Thevenin ECM cannot reproduce these effects.

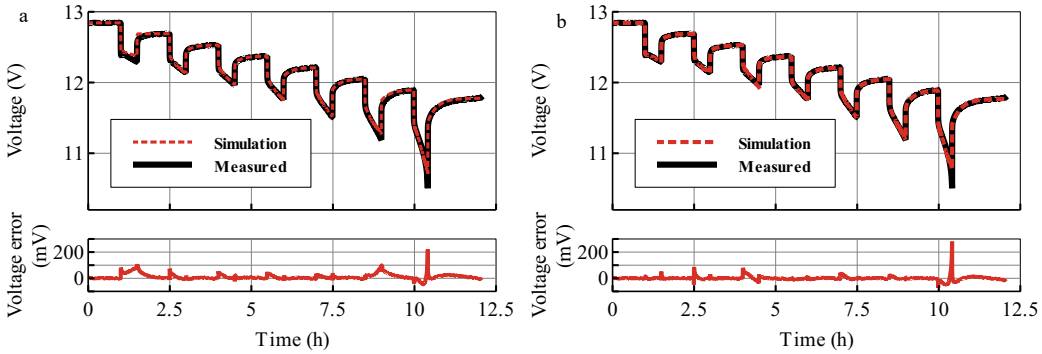

Figure 7. Parameter estimation process for the SLA battery. (**a**) Initial Parameter estimation using the linear least-square method, (**b**) Final Parameter estimation using nonlinear-least square optimization.

3. SoC Estimation

The SoC of the SLA battery and the LFP battery was estimated using two methods based on the ECMs presented before. The first method consists of a KF that estimates the states of the RC model and the second one consists of a UKF that estimates the SoC using the Thevenin model.

3.1. RC Model with Kalman Filter

The SoC of the battery can be estimated using the RC battery ECM and a KF. Firstly, the SoC is estimated using a linear KF by estimating the voltage across the bulk capacitor V_{cb}. Since the bulk capacitor voltage models the battery OCV, this method estimates the SoC of the battery using the relationship between the battery's OCV and SoC. Figure 8a,b show the OCV vs. SoC curve for both batteries used in this research.

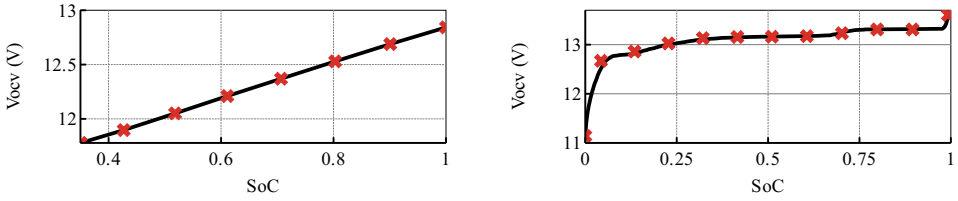

Figure 8. OCV vs. SoC curves of battery packs: (**a**) SLA battery pack. (**b**) LFP battery pack. The red markers represent the OCV points obtained with the pulse discharge test, and the black line is the curve obtained with a low current discharge test.

Since the state-space model obtained from the RC Equivalent Circuit model is linear, a linear KF can be implemented. The KF computes the optimal state estimate considering the sensors' noise and model uncertainties [36]. The KF consists of six steps that can be divided into three prediction steps and three correction steps. In the first three steps, a prediction of the state using the previous state estimation is calculated.

$$\hat{x}_k^- = A_{k-1}\hat{x}_{k-1}^+ + B_{k-1}u_{k-1}. \tag{19}$$

Then, the error covariance matrix provides information about the uncertainty of the estimation and it is computed using (20).

$$P_k^- = A_{k-1} P_{k-1}^+ A_{k-1}^T + Q. \tag{20}$$

The predicted output is calculated using the battery model and the measured current in the final prediction step:

$$\hat{y}_k = C_k \hat{x}_k^- + D_k u_k. \tag{21}$$

After finishing with the prediction steps of the KF, the Kalman gain is calculated in the first correction step:

$$K_k = P_k^+ C_k^T [C_k P_k^- C_k^T + R]^{-1}. \tag{22}$$

The state estimate is corrected using the Kalman gain and the error of the output prediction:

$$\hat{x}_k^+ = \hat{x}_k^- + K_k (y_k - \hat{y}_k). \tag{23}$$

Finally, the corrected error covariance matrix is calculated as follows:

$$P_k^+ = P_k^- - K_k [C_k P_k^- C_k^T + R] L_K^T. \tag{24}$$

The initial state estimation x_0 equals the battery OCV at 100% of SoC. A trial-and-error process tuned the measurement error covariance R and the process error covariance Q. The values of these matrices are shown in (25).

$$Q = \begin{bmatrix} 0.00001 & 0 & 0 \\ 0 & 0.001 & 0 \\ 0 & 0 & 0.9 \end{bmatrix}; R = 0.8 \tag{25}$$

Figure 9 shows a summary of the six-step algorithm needed to implement a KF.

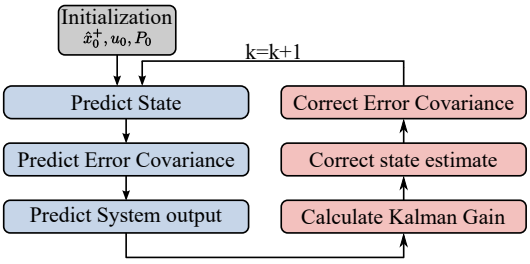

Figure 9. General steps of a KF.

3.2. Thevenin Model with Two RC Circuits with UKF

The Thevenin model with two RC circuits can be used to overcome the limitations of the RC model when estimating the SoC of LFP batteries. Since the equations presented in Section 2 show that the Thevenin model is not linear, the UKF was used to estimate the SoC of the battery to provide better estimation results for systems with a high degree of nonlinearity [37,38]. The UKF represents the uncertain variables using sigma points. The calculation of these sigma points adds more computational complexity to the SoC estimation algorithm. The UKF was implemented using MATLAB/Simulink. First, the $2N + 1$ input sigma points are calculated:

$$\mathcal{X}_{k-1} = \left[\hat{x}_{k-1}, \hat{x}_{k-1} + \gamma \sqrt{\mathbf{P}_{k-1}}, \hat{x}_{k-1} - \gamma \sqrt{\mathbf{P}_{k-1}} \right] \tag{26}$$

where γ is a constant parameter that can be tuned to improve the performance of the UKF; it depends on the number of states N and λ

$$\gamma = \sqrt{N + \lambda}. \tag{27}$$

After computing the input sigma point, the state-prediction sigma points are computed:

$$\mathcal{X}_{i,k} = f(\mathcal{X}_{k-1}, u_k). \tag{28}$$

Then, the state prediction can be computed using the following equation:

$$\hat{x}_k^- = \sum_{i=0}^{2n+1} \alpha_i^{(m)} \mathcal{X}_{i,k} \tag{29}$$

where $\alpha_0^{(m)}$ and $\alpha_i^{(m)}$ are the weighting constants used to calculate the mean. For the UKF, they are defined as:

$$\alpha_0^{(m)} = \frac{\gamma}{N+\gamma} \tag{30}$$

$$\alpha_i^{(m)} = \frac{1}{2(N+\gamma)}. \tag{31}$$

Then the error covariance time update can be calculated using:

$$\widetilde{\mathcal{X}}_{i,k}^- = \mathcal{X}_{i,k} - \hat{x}_k^- \tag{32}$$

$$\mathbf{P}_k = \sum_{i=0}^{2n+1} \alpha_i^{(c)} (\widetilde{\mathcal{X}}_{i,k}^-)(\widetilde{\mathcal{X}}_{i,k}^-)^T \tag{33}$$

where $\alpha_0^{(c)}$ and $\alpha_i^{(c)}$ are the weighting constants used to calculate the covariance, defined as follows:

$$\alpha_0^{(c)} = \frac{\gamma}{N+\gamma}(1 - \alpha^2 + \beta) \tag{34}$$

$$\alpha_i^{(c)} = \frac{1}{2(N+9\gamma)}. \tag{35}$$

In the last prediction state, the predicted output of the system is calculated. First, the output sigma points must be obtained as follows:

$$\mathcal{Y}_{i,k} = h(\mathcal{X}_{i,k}, u_k). \tag{36}$$

Then, using the output sigma points, the output of the system can be computed:

$$\hat{y}_k = \sum_{i=0}^{2n+1} \alpha_i^{(m)} \mathcal{Y}_{i,k}. \tag{37}$$

After finishing with the prediction steps, the Kalman gain can be calculated as follows:

$$\mathbf{P}_{\widetilde{y}} = \sum_{i=0}^{2n+1} (\mathcal{Y}_{i,k} - \hat{y}_k)(\mathcal{Y}_{i,k} - \hat{y}_k)^T \tag{38}$$

$$\mathbf{P}_{\widetilde{x},\widetilde{y}} = \sum_{i=0}^{2n+1} (\mathcal{X}_{i,k} - \hat{x}_k)(\mathcal{Y}_{i,k} - \hat{y}_k)^T \tag{39}$$

$$L_k = \mathbf{P}_{\widetilde{y}} \mathbf{P}_{\widetilde{x},\widetilde{y}}. \tag{40}$$

With the calculated estimator gain, the state estimate measurement is updated:

$$\hat{x}_k^+ = \hat{x}_k^- + L_k(y_k - \hat{y}_k). \tag{41}$$

Finally, the error covariance measurement is updated:

$$\mathbf{P}_k = \mathbf{P}_k - L_k \mathbf{P}_{\widetilde{y}} L_k^T. \tag{42}$$

4. SoC Estimation Results

The two batteries (SLA and LFP) were discharged using an agricultural robot mobile platform to validate the performance of the two SoC estimation methods implemented in this study. This platform is a differential wheeled agricultural robot intended to be used as a seeder robot, which consists of two 12 V Motors with a peak power of 514 W and a seeder that can be deployed using two linear actuators. The tests were performed in an indoor environment. The robot was controlled using and Radio Control transmitter to move forward and backward under flat and sloping surfaces. During each test, the battery's current and voltage information is stored in a time series database using a STM32F411CEU6 to capture the sensors' data and a Raspberry Pi 4 as the database server. Wheel speeds in RPM and acceleration data from the inertial measurement unit are also stored in the database. Then the data are processed and the SoC is estimated in simulations using MATLAB and Simulink. The components of the robot are presented in Table 2. In addition, the two model-based SoC estimation methods are compared with the Coulomb counting method performed using a Hall effect current sensor (CAS25-NP by LEM) with an accuracy of 0.8% at 25 °C and 2.5% at 85 °C. The discharge tests were performed at ambient temperature. Since the error was integrated over time, the maximum error at the end of the estimation is 83 mAh for the test performed for the SLA battery. Considering the total battery capacity of 5000 mAh, the maximum error at the end of the estimation is small, representing an error of 1.6% for the reference SoC. The current and voltage data obtained for both batteries are presented in Figure 10a,b.

Table 2. Components of the agricultural robot mobile platform.

Element	Description
Inertial measurement unit	MPU-6050
Wheel Encoders	US Digital E3-500-375-NE-E-D-3
Microcontroller	STMicroelectronics STM32F411CEU6
Motor Controller	Ampflow AF160
Motors	Ampflow E30-150-12-G16
Linear Actuators	Firgelli Automations FA-OS-240-12-6
SLA Battery	AJC 12 V 5 Ah
LFP Battery	RoyPow 12 V 6 Ah
Current Sensor	LEM CAS 25-NP

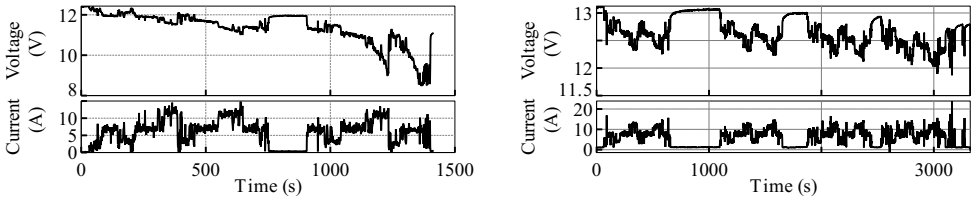

Figure 10. Measured current and voltage during tests with the robotic platform. (**a**) SLA battery pack. (**b**) LFP battery pack.

4.1. SLA Battery Pack

Regarding the performance of the SoC estimation for the SLA battery using the RC model with KF, Figure 11a presents the convergence of the filter to the SoC provided by the current measurement. Although the initial estimation error is about 20%, the filter converges to the reference SoC value after 500 s. The results of the SoC estimation, performed using the Thevenin model with two RC networks and the UKF, show a higher accuracy across all SoC levels. Regarding the voltage estimation for the SLA battery, the voltage estimation error using the Thevenin model is higher than the RC model, as depicted in Figure 11b. This model mismatch affected the convergence to the reference SoC when the initial SoC estimation error is about 10%, as illustrated in Figure 12.

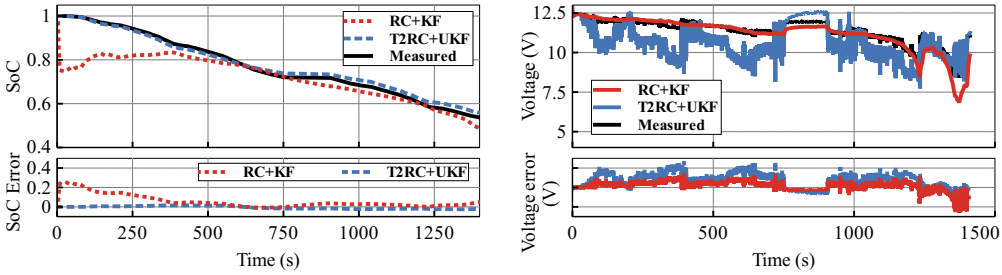

Figure 11. Method performance validation using robot operation data for the SLA battery: (**a**) SoC estimation performance of the RC model with KF (RC+KF) and the 2 RC Thevenin model with UKF (T2RC+UKF). (**b**) Comparison of battery voltage estimation performance of RC model with KF (RC+KF) and the 2 RC Thevenin model with UKF (T2RC+UKF).

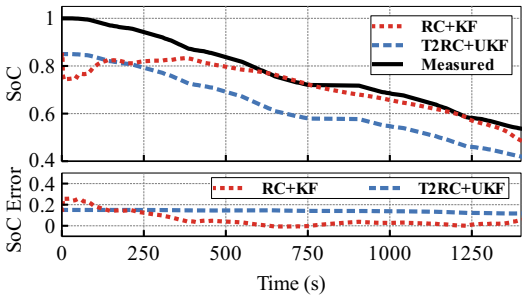

Figure 12. RC model with KF (RC+KF) and the 2 RC Thevenin model with UKF (T2RC+UKF) convergence test under wrong SoC initialization for the SLA battery.

4.2. LFP Battery Pack

The battery SoC and voltage estimation results for the LFP battery pack SoC estimation are shown in Figure 13a,b. Although the voltage estimation using the RC model performs well in all SoC levels, the SoC estimation using the RC model and the KF method works only for low SoC levels. The performance of this method for the LFP battery can be explained by analyzing the OCV vs. SoC curve, which has two low slope regions. The first one starts at 98% and ends at 75% of the SoC, where the voltage change is approximately 0.024 V. Moreover, the voltage changes from 65% to 25% of the battery SoC is lower than 0.2 V. Therefore, since this method relies on the OCV vs. SoC curve, small errors in the battery's OCV estimation will produce significant errors in the final SoC estimation. Regarding the results of the SoC estimation using the Thevenin model and the UKF, the error is reduced since this model considers the SoC as a state. Then the utilization of the Thevenin model with two RC circuits with the UKF can overcome the limitations on the flat regions of the OCV vs. SoC curve for this battery.

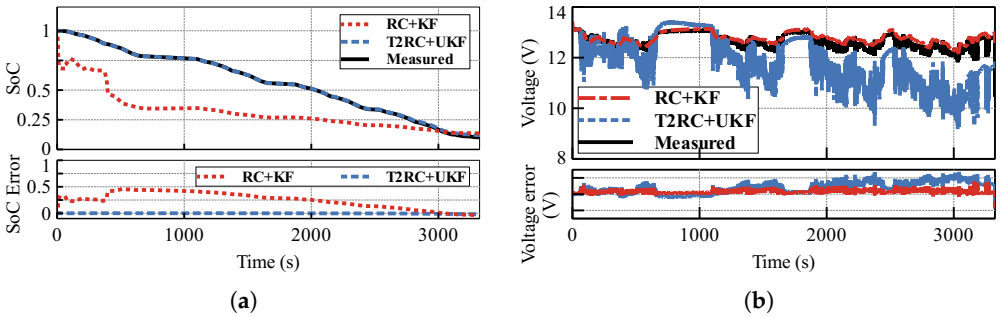

Figure 13. Method performance validation using robot operation data for the LFP battery pack: (**a**) SoC estimation performance of the RC model with KF (RC+KF) and the 2 RC Thevenin model with UKF (T2RC+UKF). (**b**) Comparison of battery voltage estimation performance of RC model with KF (RC+KF) and the 2 RC Thevenin model with UKF (T2RC+UKF).

4.3. Managerial Impacts

The results of this work show that SoC estimation methods intended for other applications, such as EVs, may not perform appropriately for agricultural robot applications because of the hardware and cost constraints presented in agricultural robots. Therefore, developing new SoC estimation techniques intended for agricultural robots is still needed to increase the presence of robots on farms. Further efforts are needed to implement and validate these techniques in agricultural robot applications. Moreover, the lack of accurate SoC estimation methods makes implementing robots in agriculture difficult because the robots' safe and continuous operation cannot be ensured and the energy consumption of robots cannot be optimized, reducing efficiency.

5. Conclusions

This study analyzed the performance of two model-based SoC estimation methods for SLA and LFP batteries using voltage and current measurements obtained using low-cost measurement devices appropriated for small agricultural robots. The batteries were discharged until the maximum depth of discharge to analyze the accuracy and convergence of the methods in a wider SoC range. The SoC estimation using the RC model with Kalman Filter (RC model with KF) demonstrated satisfactory performance for the SLA battery with a maximum error of 5% and a mean absolute error (MAE) of 2.2% after convergence. In addition, this method provides convergence to the reference SoC even if an incorrect initial estimation has been performed. However, the SoC estimation using the RC model with KF for the LFP battery performed poorly due to the broad flat region in the OCV vs. SoC curve of this battery.

In contrast to the method based on the RC model, the method based on the Thevenin model with two RC circuits with Unscented Kalman Filter (T2RC model with UKF) offered good performance for the two types of batteries used in this study. The mean absolute errors for the SLA and LFP batteries were 0.27% and 0.5%, respectively. In battery packs for mobile robots, the estimation accuracy using this method was affected under incorrect initialization because the estimation did not converge to the reference SoC. If the battery has reached a stable state after several minutes of rest, the OCV method can be used to obtain an accurate estimation; however, in the case of LFP batteries, the measurement accuracy should be high to obtain a good initial estimation. On the other hand, two models can be used during battery operation: one for continuous SoC estimation and another for SoC initialization and correction. Regarding the results of this research, the Thevenin model could be used for continuous operation and the RC model for SoC initialization and correction.

Finally, the limitations of the methods presented in this work must be considered for the design of full-range SoC estimation systems used in agricultural mobile robots. For obtaining a more rigorous evaluation, the models should include non-modeled parameters such as battery aging and temperature, improving the estimation accuracy in farm environments where the temperature varies during operation and batteries are not replaced periodically. Moreover, the performance of the SoC estimation algorithms implemented in a low-cost microcontroller with low computational power for agricultural robot applications should be validated.

Author Contributions: Conceptualization, G.M., A.C. and D.A.-B.; methodology, G.M. and A.C.; software, G.M.; validation, G.M. and A.C.; formal analysis, G.M., A.C. and D.A.-B.; investigation, G.M. and A.C.; writing—review and editing, G.M., A.C. and D.A.-B.; supervision, A.C. and W.M.; funding acquisition, A.C. and W.M. All authors have read and agreed to the published version of the manuscript.

Funding: This research received no external funding.

Institutional Review Board Statement: Not applicable.

Informed Consent Statement: Not applicable.

Data Availability Statement: Data available on request.

Acknowledgments: The authors would like to thank the Ministère des Relations Internationales et de la Francophonie du Quebec, MRIF, Quebec, for the financial support.

Conflicts of Interest: The authors declare no conflict of interest.

References

1. Canada Energy Regulator. *Canada Energy Future 2020*; Canada Energy Regulator: Calgary, AB, Canada, 2020; p. 100.
2. FAO. *Food and Agriculture Organization of the United Nations*; FAO: Rome, Italy, 2022; pp. 342–342. [CrossRef]
3. Longo, F.; Mirabelli, G.; Solina, V.; Belli, L.; Abdallah, C.B.; Ben-Ammar, O.; Bottani, E.; García-Gallego, J.M.; Germanos, M.; González, F.J.M.; et al. An overview of approaches and methodologies for supporting smallholders: ICT tools, blockchain, business models, sustainability indicators, simulation models. *Procedia Comput. Sci.* **2023**, *217*, 1930–1939. [CrossRef]
4. Christiaensen, L.; Rutledge, Z.; Taylor, J.E. Viewpoint: The future of work in agri-food. *Food Policy* **2021**, *99*, 101963. [CrossRef]
5. Tian, H.; Wang, T.; Liu, Y.; Qiao, X.; Li, Y. Computer vision technology in agricultural automation—A review. *Inf. Process. Agric.* **2020**, *7*, 1–19. [CrossRef]
6. Ghobadpour, A.; Monsalve, G.; Cardenas, A.; Mousazadeh, H. Off-Road Electric Vehicles and Autonomous Robots in Agricultural Sector: Trends, Challenges and Opportunities. *Vehicles* **2022**, *4*, 843–864. [CrossRef]
7. Oliveira, L.F.; Moreira, A.P.; Silva, M.F. Advances in agriculture robotics: A state-of-the-art review and challenges ahead. *Robotics* **2021**, *10*, 52. [CrossRef]
8. Sparrow, R.; Howard, M. Robots in agriculture: Prospects, impacts, ethics and policy. *Precis. Agric.* **2021**, *22*, 818–833. [CrossRef]
9. Gonzalez-de Santos, P.; Fernández, R.; Sepúlveda, D.; Navas, E.; Emmi, L.; Armada, M. Field Robots for Intelligent Farms—Inhering Features from Industry. *Agronomy* **2020**, *10*, 1638. [CrossRef]
10. Gan, N.; Sun, Z.; Zhang, Z.; Xu, S.; Liu, P.; Qin, Z. Data-Driven Fault Diagnosis of Lithium-Ion Battery Overdischarge in Electric Vehicles. *IEEE Trans. Power Electron.* **2022**, *37*, 4575–4588. [CrossRef]
11. Lyu, N.; Jin, Y.; Xiong, R.; Miao, S.; Gao, J. Real-time overcharge warning and early thermal runaway prediction of Li-ion battery by online impedance measurement. *IEEE Trans. Ind. Electron.* **2021**, *69*, 1929–1936. [CrossRef]
12. Monsalve, G.; Cardenas, A.; Martinez, W. Analysis of two Equivalent Circuit Models for State of Charge Estimation using Kalman Filters. In Proceedings of the 2022 IEEE 31st International Symposium on Industrial Electronics (ISIE), Anchorage, AK, USA, 1–3 June 2022; pp. 347–353. [CrossRef]
13. Ng, K.S.; Moo, C.S.; Chen, Y.P.; Hsieh, Y.C. Enhanced coulomb counting method for estimating state-of-charge and state-of-health of lithium-ion batteries. *Appl. Energy* **2009**, *86*, 1506–1511. [CrossRef]
14. Xiong, R.; Cao, J.; Yu, Q.; He, H.; Sun, F. Critical Review on the Battery State of Charge Estimation Methods for Electric Vehicles. *IEEE Access* **2017**, *6*, 1832–1843. [CrossRef]
15. Chemali, E.; Kollmeyer, P.J.; Preindl, M.; Ahmed, R.; Emadi, A. Long Short-Term Memory Networks for Accurate State-of-Charge Estimation of Li-ion Batteries. *IEEE Trans. Ind. Electron.* **2018**, *65*, 6730–6739. [CrossRef]
16. Chemali, E.; Kollmeyer, P.J.; Preindl, M.; Emadi, A. State-of-charge estimation of Li-ion batteries using deep neural networks: A machine learning approach. *J. Power Sources* **2018**, *400*, 242–255. [CrossRef]
17. How, D.N.; Hannan, M.A.; Lipu, M.S.; Sahari, K.S.; Ker, P.J.; Muttaqi, K.M. State-of-Charge Estimation of Li-Ion Battery in Electric Vehicles: A Deep Neural Network Approach. *IEEE Trans. Ind. Appl.* **2020**, *56*, 5565–5574. [CrossRef]
18. Bhangu, B.S.; Bentley, P.; Stone, D.A.; Bingham, C.M. Nonlinear observers for predicting state-of-charge and state-of-health of lead-acid batteries for hybrid-electric vehicles. *IEEE Trans. Veh. Technol.* **2005**, *54*, 783–794. [CrossRef]
19. Ahmed, R.; Gazzarri, J.; Onori, S.; Habibi, S.; Jackey, R.; Rzemien, K.; Tjong, J.; Lesage, J. Model-Based Parameter Identification of Healthy and Aged Li-ion Batteries for Electric Vehicle Applications. *SAE Int. J. Altern. Powertrains* **2015**, *4*, 233–247. [CrossRef]
20. Vasebi, A.; Bathaee, S.M.; Partovibakhsh, M. Predicting state of charge of lead-acid batteries for hybrid electric vehicles by extended Kalman filter. *Energy Convers. Manag.* **2008**, *49*, 75–82. [CrossRef]
21. Partovibakhsh, M.; Liu, G. An adaptive unscented kalman filtering approach for online estimation of model parameters and state-of-charge of lithium-ion batteries for autonomous mobile robots. *IEEE Trans. Control. Syst. Technol.* **2015**, *23*, 357–363. [CrossRef]
22. Hu, X.; Sun, F.; Zou, Y. Estimation of state of charge of a Lithium-Ion battery pack for electric vehicles using an adaptive luenberger observer. *Energies* **2010**, *3*, 1586–1603. [CrossRef]
23. Hu, X.; Li, S.; Peng, H. A comparative study of equivalent circuit models for Li-ion batteries. *J. Power Sources* **2012**, *198*, 359–367. [CrossRef]
24. He, Z.; Yang, Z.; Cui, X.; Li, E. A Method of State-of-Charge Estimation for EV Power Lithium-Ion Battery Using a Novel Adaptive Extended Kalman Filter. *IEEE Trans. Veh. Technol.* **2020**, *69*, 14618–14630. [CrossRef]
25. Hossain, M.; Haque, M.E.; Arif, M.T. Online Model Parameter and State of Charge Estimation of Li-Ion Battery Using Unscented Kalman Filter Considering Effects of Temperatures and C-Rates. *IEEE Trans. Energy Convers.* **2022**, *37*, 2498–2511. [CrossRef]
26. Misyris, G.S.; Doukas, D.I.; Papadopoulos, T.A.; Labridis, D.P.; Agelidis, V.G. State-of-Charge Estimation for Li-Ion Batteries: A More Accurate Hybrid Approach. *IEEE Trans. Energy Convers.* **2019**, *34*, 109–119. [CrossRef]

27. Zhang, F.; Liu, G.; Fang, L.; Wang, H. Estimation of battery state of charge with H∞ observer: Applied to a robot for inspecting power transmission lines. *IEEE Trans. Ind. Electron.* **2012**, *59*, 1086–1095. [CrossRef]
28. Rivera-Barrera, J.P.; Muñoz-Galeano, N.; Sarmiento-Maldonado, H.O. Soc estimation for lithium-ion batteries: Review and future challenges. *Electronics* **2017**, *6*, 102. [CrossRef]
29. Wang, Q.; Wang, J.; Zhao, P.; Kang, J.; Yan, F.; Du, C. Correlation between the model accuracy and model-based SOC estimation. *Electrochim. Acta* **2017**, *228*, 146–159. [CrossRef]
30. Johnson, V.H.; Pesaran, A.A.; Court, B. Temperature-Dependent Battery Models for High-Power Lithium-Ion Batteries. In Proceedings of the 17th Annual Electric Vehicle Symposium, Montreal, QC, Canada, 16–18 October 2000.
31. Chan, H.L.; Sutanto, D. A new battery model for use with battery energy storage systems and electric vehicles power systems. In Proceedings of the 2000 IEEE Power Engineering Society Winter Meeting, Singapore, 23–27 January 2000; Volume 1, pp. 470–475. [CrossRef]
32. Hossain, M.; Member, S.; Saha, S.; Arif, M.T.; Haque, E.; Member, S. A Parameter Extraction Method for the Li-Ion Batteries With Wide-Range Temperature Compensation. *IEEE Trans. Ind. Appl.* **2020**, *56*, 5625–5636. [CrossRef]
33. Xiong, R.; Sun, F.; He, H. State-of-charge estimation of lithium-ion batteries in electric vehicles based on an adaptive extended Kalman filter. *Gaojishu Tongxin/Chin. High Technol. Lett.* **2012**, *22*, 198–204. [CrossRef]
34. Song, Q.; Mi, Y.; Lai, W. A Novel Variable Forgetting Factor Recursive Least Square Algorithm to Improve the Anti-Interference Ability of Battery Model Parameters Identification. *IEEE Access* **2019**, *7*, 61548–61557. [CrossRef]
35. Plett, G.L. Equivalent Circuit Models. In *Battery Management Systems, Volume 1—Battery Modeling*; Artech House: Norwood, MA, USA, 2015; Chapter 2.
36. Plett, G.L. Battery-State Estimation. In *Battery Management Systems, Volume II: Equivalent-Circuit Methods*; Artech House Publishers: Norwood, MA, USA, 2015; Chapter 3.
37. Shehab El Din, M.; Hussein, A.A.; Abdel-Hafez, M.F. Improved battery SOC estimation accuracy using a modified UKF with an adaptive cell model under real EV operating conditions. *IEEE Trans. Transp. Electrif.* **2018**, *4*, 408–417. [CrossRef]
38. Wu, X.; Li, X.; Du, J. State of Charge Estimation of Lithium-Ion Batteries over Wide Temperature Range Using Unscented Kalman Filter. *IEEE Access* **2018**, *6*, 41993–42003. [CrossRef]